Trans. Mat. Res. Soc. Japan 41[1] 101-108 (2016)

Substitution effect of tetravalent and pentavalent elements on thermoelectric properties in In_2O_3-SnO_2 system

Rintaro Abe, Hiroyuki Fujishiro* and Tomoyuki Naito
Faculty of Engineering, Iwate University, Morioka 020-8551, Japan
* Corresponding author: Fax: 81-19-621-6363, and/or e-mail: fujishiro@iwate-u.ac.jp

Thermoelectric properties of $In_{2-x}M_xO_3$ system doped with tetravalent metal (M) ions (Si^{4+}, Ti^{4+}, Ge^{4+}, Sn^{4+}, Te^{4+}, and Ce^{4+}) were investigated at temperatures up to 1273 K. For the Ge-substituted system, the power factor P takes a maximum of 9.5×10^{-4} W/K^{2}m around 1150 K and dimensionless thermoelectric figure of merit ZT shows a maximum of 0.18 at 1000 K for the x=0.025 sample, which is the solubility limit of Ge. The maximum ZT of the $In_{1.9}M_{0.1}O_3$ series was about 0.13 around 1000 K for the Si^{4+}, Ge^{4+} and Sn^{4+} doped samples. We also investigated the thermoelectric properties of the In_2O_3-SnO_2 system doped with pentavalent Sb element to replace the expensive In_2O_3 to the plentiful SnO_2. The Sb atom was preferentially substituted for the In-site and the thermoelectric properties do not exceed those of pure In_2O_3. The potential of the thermoelectric properties in the doped In_2O_3-SnO_2 system was discussed.

Key words: thermoelectric material, In_2O_3, SnO_2, spark plasma sintering, dimensionless figure of merit, power factor

1. INTRODUCTION

The thermoelectric technology using waste heat for power generation devices has been revived because of the recent energy crisis together with other renewable energy sources. Since the discovery of $NaCo_2O_4$ in 1997 [1], oxide thermoelectric materials have been intensively studied, as a substitute for conventional intermetallic thermoelectric materials using heavy metal series such as Bi_2Te_3 [2-4]. Despite their lower performance as compared to the intermetallic materials, oxides are very attractive for high temperature applications due to their chemical stability in air.

Recently, doped indium oxide (In_2O_3) compounds are reported to exhibit relatively high thermoelectric performances. The substitution of Ge for In was reported to decrease the electrical resistivity and, at the same time, the precipitation of fine particles of the $In_2Ge_2O_7$ impurity phase efficiently reduced the thermal conductivity, resulting in the higher dimensionless figure of merit of ZT=0.45 at 1273 K in air (=$S^2T/\rho\kappa$, S: Seebeck coefficient, T: absolute temperature, ρ: electrical resistivity, and κ: thermal conductivity) in the $In_{1.8}Ge_{0.2}O_3$ system [5]. The single element substitution of Co [6], Sn [7], and co-substitution of Zn+Nd [8], Zn+Ge [9], Zn+Ce [10], M+Sn (M=Zn, Cu, Ni) [11] for the indium site has been recently investigated and ZT values as high as 0.3 can be obtained at high temperatures. The approaches of fine-grained and high packing were also performed to decrease the thermal conductivity [12, 13]. However, systematic study of the single element substitution for the indium site has not investigated yet, and the reason why the Ge-substituted In_2O_3 shows the higher ZT value, has not clarified compared to other element substitution.

In this study, we investigated the In_2O_3 polycrystals doped with various tetravalent elements (Si, Ti, Ge, Sn, Te and Ce) and measured the electrical and thermal properties. The better effect of the Ge-doping on the thermoelectric properties in In_2O_3 system was discussed.

In order to reduce the amount of In as a rare metal element, we also investigated thermoelectric properties of the In_2O_3-SnO_2 system doped with pentavalent Sb element. Because SnO_2 shows similar physical properties to In_2O_3, which is inexpensive, plentiful and nontoxic, as a substitute for the expensive In_2O_3. The Sb^{5+} doping is expected to perform as a donor by both the In^{3+}- and Sn^{4+}-site substitutions simultaneously. The potential of the In_2O_3-SnO_2 system was discussed as a thermoelectric material.

2. EXPERIMENTAL PROCEDURE

$In_{2-x}Ge_xO_3$ ($0 \leq x \leq 0.3$), $In_{1.9}M_{0.1}O_3$ (M=Si, Ti, Ge, Sn, Te, Ce) and Sb-doped In_2O_3-SnO_2 systems were prepared by the spark plasma sintering (SPS) method. In_2O_3 (99.9%), SiO_2 (99.9%), TiO_2 (99.99%), GeO_2 (99.99%), SnO_2 (99.9%), TeO_2 (99.9%), CeO_2 (99.9%) and Sb_2O_5 (99.99%) fine powders were used as raw materials. The powders were mixed with stoichiometoric ratio for 1 h by automatic mortar and were sintered by the SPS apparatus (NJS-LABOX-110C) at about 1273 K for 5-10 min in vacuum. The sintered bulks were cut into rectangles and annealed at 1173 K in air for 2 h to reduce oxygen defects. Powder X-ray diffraction (XRD) measurements were performed (Rigaku Multi Flex) at room temperature using Cu $K\alpha$ radiation in the range of $20° \leqq 2\theta \leqq 90°$ with 0.02° steps, and the lattice parameters were determined using a Rietveld refinement program, RIETAN 2000 [14]. Scanning electron

microscope (SEM) images were taken and quantitative element analyses were performed by electron probe micro-analyzer (EPMA). The electrical resistivity $\rho(T)$ (or electrical conductivity $\sigma(T)=1/\rho(T)$) and Seebeck coefficient $S(T)$ were simultaneously measured in the temperature range from 300 to 1273 K using an automated measuring system (Ozawa Science RZ2001i) and the thermoelectric power factor $P=S^2/\rho$ was calculated. The thermal conductivity $\kappa(T)$ was measured by a laser flash method (Ulvac-Riko TC-7000) from 300 K to 1023 K. The κ value below 300 K was also measured by steady-state heat flow method using home-made measuring system [15]. A dimensionless figure of merit $ZT=S^2T/\rho\kappa$ was estimated using these values. Hall effect experiments were carried out by five-terminal method at room temperature to determine the carrier concentration n and Hall mobility μ, which was calculated by $\mu=\sigma|R_H|$ (R_H: Hall coefficient).

3. RESULTS AND DISCUSSION

3.1 $In_{2-x}Ge_xO_3$ ($0\le x\le 0.3$)

Figure 1 shows the XRD patterns of the $In_{2-x}Ge_xO_3$ system ($0\le x\le 0.3$). The impurity peaks of $In_2Ge_2O_7$ appeared for $x\ge 0.05$. Berardan *et al*. reported that the solubility limit of Ge in In_2O_3 was about $x=0.01$~0.02 by conventional solid-state reaction method [5], which was slightly lower than that of our samples. The increase of the solubility limit in our samples may result from the difference in the fabricating method.

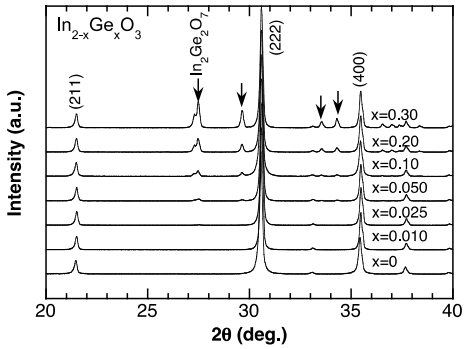

Fig. 1. XRD patterns of $In_{2-x}Ge_xO_3$ ($0\le x\le 0.3$). Arrows indicate the $In_2Ge_2O_7$ impurity peaks.

Figure 2 presents the temperature dependence of the electrical resistivity ρ, the Seebeck coefficient S and the power factor P of $In_{2-x}Ge_xO_3$ ($0\le x\le 0.3$). ρ and $|S|$ values decreased with increasing x up to $x=0.05$ and then slightly increased with increasing x. These results suggest that electron was doped by the Ge substitution up to the solubility limit. The decrease of the $|S|$ value accompanied by the decrease of the ρ value is a general trend in condensed matter. The power factor of the $x=0.025$ sample showed the maximum value of about 9.5×10^{-4} W/K^{2}m around 1150 K.

Figure 3 presents the carrier concentration n and the Hall mobility μ of $In_{2-x}Ge_xO_3$ at room temperature, as a function of x. The n value sharply increases with the increase in x, takes a maximum of 3.2×10^{20} cm^{-3} at $x=0.025$, and then slightly decreases with increasing x. The Hall mobility μ decreased sharply with increasing x up to $x=0.025$ due to the Ge substitution for the In site and then gradually decreased due to the increase of the scattering by $In_2Ge_2O_7$ precipitates.

Figure 4(a) shows the temperature dependence of the thermal conductivity κ of the $In_{2-x}Ge_xO_3$ system. For the pure In_2O_3, $\kappa(T)$ is inversely proportional to T, which results from phonon-phonon scattering. The κ value at 300 K decreased with increasing Ge contents x and $\kappa(T)$ of the Ge-substituted samples is less temperature dependent, which may come from the phonon scattering by $In_2Ge_2O_7$ impurity particles. Figure 4(b) depicts the temperature dependence of dimensionless figure of merit ZT of the $In_{2-x}Ge_xO_3$ system. The ZT value increases with increasing T and that of the Ge-substituted samples is larger than that of pure In_2O_3 at high temperatures. The maximum ZT value was 0.18 at 1023 K for the $x=0.025$ sample, which was smaller than the reported values for the $In_{2-x}Ge_xO_3$ system; $ZT=0.3$ for the $x=0.2$ sample was interpolated at 1000 K from the Berardan's data [5].

Figure 5 shows the ZT and P values at 1000 K, as a function of x. Both ZT and P values take a maximum at the same x of 0.025, which is the solubility limit of Ge in In_2O_3. The $x=0.025$ sample shows the best thermoelectric performance both electrically and thermally in the $In_{2-x}Ge_xO_3$ system. We compare our results of the $x=0.025$ sample at 1000 K to those of the $x=0.2$ sample at 1000 K by Berardan *et al.* [5]. The P value of our sample (=0.95 mW/K^{2}m) is larger than that

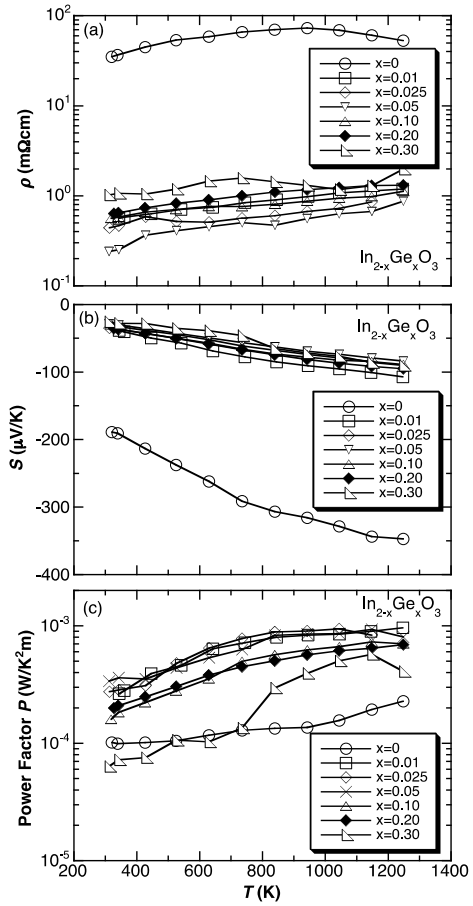

Fig. 2. Temperature dependence of the (a) electrical resistivity ρ, (b) Seebeck coefficient S and (c) power factor P of $In_{2-x}Ge_xO_3$ ($0\le x\le 0.3$).

(=0.45 mW/K^{2}m) of the Berardan's sample, which suggests that the electrical property of our samples is better. However, the thermal conductivity κ of our sample (=52 mW/cmK) is about three times larger than that (=16 mW/cmK) of the Berardan's sample. The reduction of the κ value of our samples is a possible solution to enhance the *ZT* value.

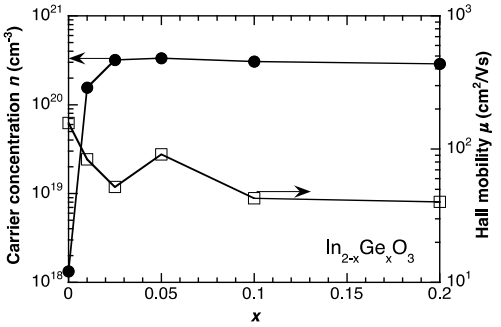

Fig. 3. Carrier concentration n and Hall mobility μ of $In_{2-x}Ge_xO_3$ at room temperature, as a function of the contents x of Ge.

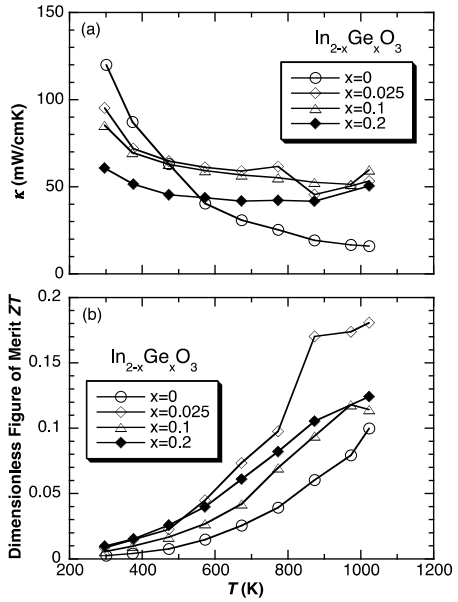

Fig. 4 Temperature dependence of the (a) thermal conductivity κ and (b) of dimensionless figure of merit *ZT* of the $In_{2-x}Ge_xO_3$ system.

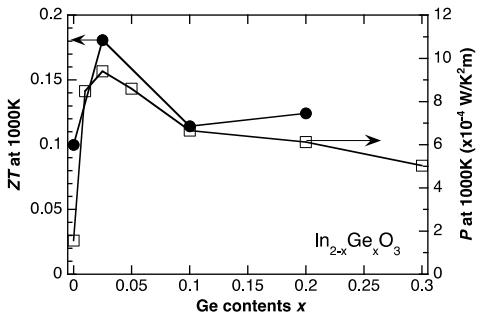

Fig. 5 the *ZT* and *P* values at 1000 K, as a function of contents of Ge, x in $In_{2-x}Ge_xO_3$.

3.2 $In_{1.9}M_{0.1}O_3$ (M=Si, Ti, Ge, Sn, Te, Ce)

In the previous subsection, the *P* and *ZT* values took a maximum at x=0.025 for the $In_{2-x}Ge_xO_3$ system. On the other hand, these values by Berardan *et al.* slightly increased with increasing x at each temperature [5]. Since the solubility limit and the particle size of the impurity phase seem to change depending on the doped element, the thermoelectric properties of $In_{1.9}M_{0.1}O_3$ doped with various tetravalent M ions were investigated for the x=0.1 impurity concentration, which is higher than the solubility limit of Ge in In_2O_3 in this study.

Figure 6 shows the XRD patterns of $In_{1.9}M_{0.1}O_3$ (M=Si, Ti, Ge, Sn, Te, Ce). The impurity peak of the $In_4Si_5O_{12}$, In_2TiO_5, $In_2Ge_2O_7$, SnO_2 and CeO_2 were detected for the M=Si, Ti, Ge, Sn, Ce samples, respectively, which were also confirmed by the quantitative analysis by EPMA shown in the later. In the $In_{1.9}Te_{0.1}O_3$ sample, there was no impurity peaks.

Figures 7(a) and 7(b) present the SEM images and the characteristic X-ray images of each doped element in the $In_{1.9}M_{0.1}O_3$ samples, respectively. The distribution of the impurity phases depends on the substituted M ions; in the $In_{1.9}Ge_{0.1}O_3$ sample, the $In_2Ge_2O_7$ particles as large as about 50 μm were precipitated, and the grain size of the impurity phase in the M=Sn, Ce samples was about 10~30 μm. On the other hand, the impurity phase in the M=Si, Ti, Te samples was finely and uniformly distributed.

Figure 8 presents the temperature dependence of the ρ, S and P values of the $In_{1.9}M_{0.1}O_3$ samples. Compared to the pure In_2O_3, the ρ and S values of the M=Ge and Sn samples drastically decreased due to the carrier doping. The ρ and S values of the M=Si and Ti samples decreased moderately. The relationship between the ρ and S values and the particle size of the impurity phase shown in Fig. 7 does not necessarily seem to correlate with each other, which is remained for further study. In Fig. 8(c), the power factor P of the Ge-doped sample shows the maximum value of 7.3×10^{-4} W/K^{2}m at 1148 K. in the $In_{1.9}M_{0.1}O_3$ system.

Table I summarizes the carrier concentration n, electrical conductivity σ and Hall mobility μ of the $In_{1.9}M_{0.1}O_3$ samples at room temperature. σ was calculated using the relation of $\sigma=en\mu$. The Ge- and Sn-doped samples showed higher carrier concentration n and, at the same time, relatively higher Hall mobility μ, which generally decreases with increasing n value due to the increase of the scattering by carriers. The size and the distribution of impurity particles also might influence on the electrical conductivity, in which the carriers are scattered by grain boundaries and/or the lattice strain due to the impurity particles.

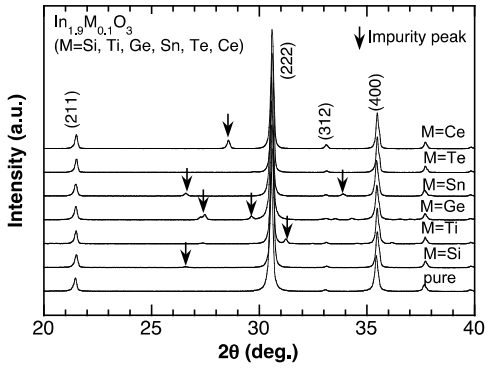

Fig. 6. XRD patterns of $In_{1.9}M_{0.1}O_3$ (M=Si, Ti, Ge, Sn, Te, Ce).

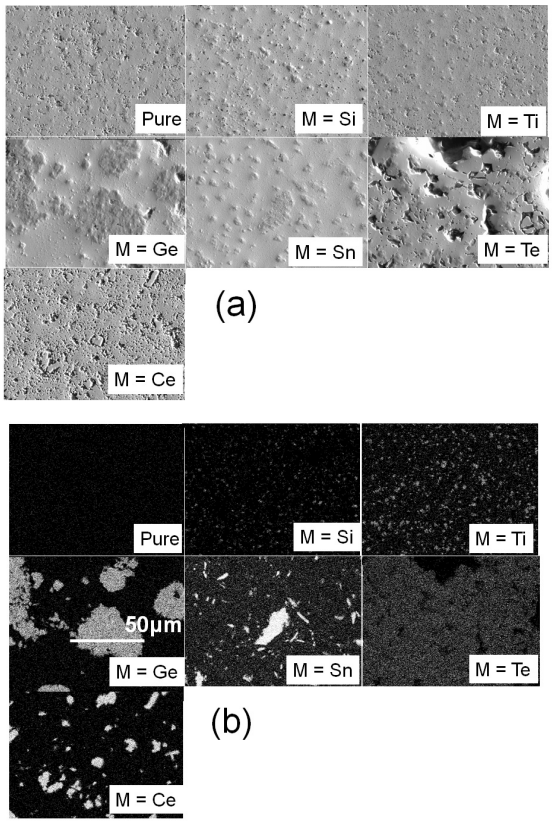

Fig. 7. (a) SEM images and (b) characteristic X-ray images of each doped element for the $In_{1.9}M_{0.1}O_3$ samples.

We investigated the influence of the substituted M ion in the $In_{1.9}M_{0.1}O_3$ system on the thermoelectric and crystallographic properties. Figure 9(a) shows the relationship between the ionic radius of the impurity M ion with coordination number (CN) of VI [16] and the lattice parameter of the $In_{1.9}M_{0.1}O_3$ samples. Indium oxide has a Bixbyite-type cubic lattice structure with *Ia*3-(206) space group [17]. The lattice parameter seems to be correlated with the ionic radius of M ion, which suggests the substitution of the M ion for the In-site, except for the M=Te and Ce samples. For the M=Te and Ce samples, the Rietveld refinement might not be successful, since the solubility may be too small.

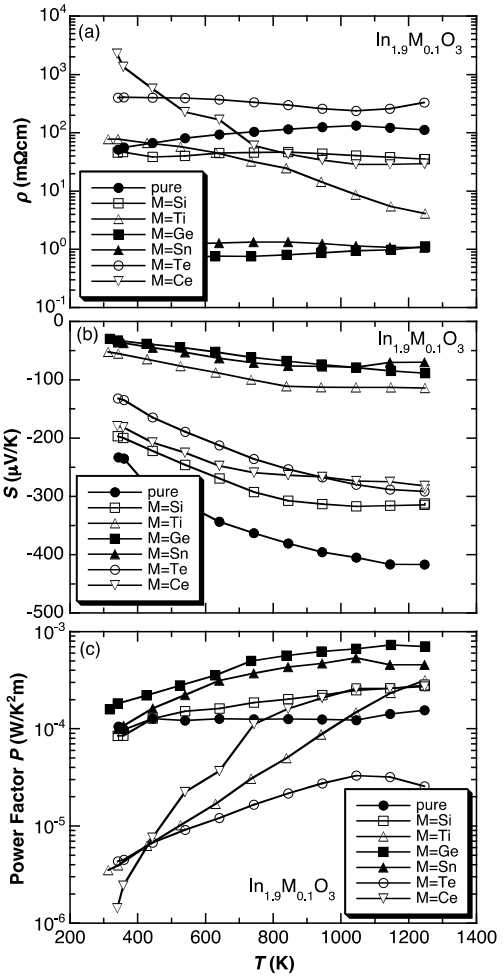

Fig. 8. Temperature dependence of ρ, S and P values of the $In_{1.9}M_{0.1}O_3$ samples.

Table I. Carrier concentration n, electrical resistivity σ and Hall mobility μ of the $In_{1.9}M_{0.1}O_3$ samples.

	Carrier concentration n (cm^{-3})	Electrical conductivity σ (S/cm)	Hall mobility μ (cm^2/Vs)
pure	1.3×10^{18}	29	157
M=Si	6.7×10^{18}	22	24
M=Ti	1.2×10^{20}	13	0.8
M=Ge	3.1×10^{20}	1780	43
M=Sn	1.8×10^{20}	116	4.9
M=Te	1.1×10^{19}	3	1.7
M=Ce	6.0×10^{18}	0.4	0.5

Figure 9(b) presents the relationship between the carrier concentration n and the Hall mobility μ of the $In_{1.9}M_{0.1}O_3$ samples. The M=Ge and Sn samples show the relatively higher n values. It should be noted that the Ge-doped sample presents the higher Hall mobility, though the carrier doping introduces the crystal defects in general. Figure 9(c) depicts the relationship between the Seebeck coefficient S and the power factor P at 1200 K of the $In_{1.9}M_{0.1}O_3$ samples. Due to the introduction of the carriers shown in Fig. 9(b), the M ion dependence of the S value at 1200 K is resemble with that of the n value. Seebeck coefficient S of a conductor is given by

$$S = \frac{\pi^2}{3}\left(\frac{k_B}{e}\right)\frac{k_B T}{\sigma}\frac{\partial\sigma(E)}{\partial E} \quad (1)$$

where E is the electron energy. Roughly speaking, $|S|$ is inversely proportional to the $\sigma=en\mu$ value. In the $In_{1.9}M_{0.1}O_3$ system, the Ge-substituted sample shows the highest power factor P, which results from the relatively higher σ value due to both higher n and μ values, and the relatively not small $|S|$ value. These properties are clear contrast with other substituted ions for the In-site.

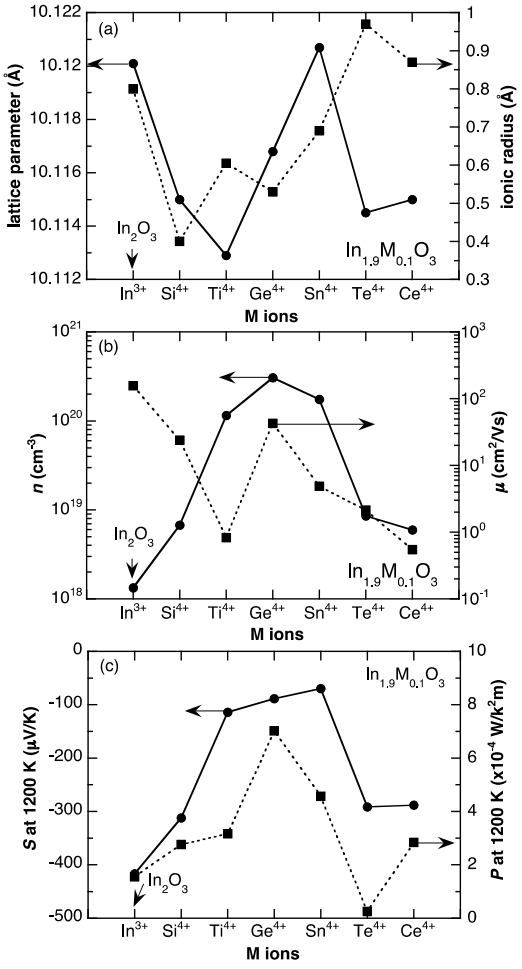

Fig. 9. The relations (a) between the lattice parameter and the ionic radius of the substituted M ion and (b) between the carrier concentration n and the Hall mobility μ and (c) between the Seebeck coefficient S and power factor P at 1200 K for each doped M ion in $In_{0.9}M_{0.1}O_3$ system.

Figure 10(a) shows the temperature dependence of the thermal conductivity κ of the $In_{1.9}M_{0.1}O_3$ (M=Si, Ti, Ge, Sn) samples. κ at 300 K was decreased by the substitution of the M ion, compared to the pure In_2O_3. κ(300 K) of the Si-doped sample was most strongly depressed in the samples. $\kappa(T)$ of the $In_{1.9}M_{0.1}O_3$ samples is less temperature dependence, which may mainly come from the phonon scattering by impurity phases and particles identified by XRD and EMPA shown in Figs. 6 and 7.

Figure 10(b) depicts the temperature dependence of dimensionless figure of merit ZT. The ZT value increases with increasing T. The $In_{1.9}M_{0.1}O_3$ samples doped by Ge, Sn and Si shows the higher ZT values than that of the pure In_2O_3 sample. The maximum ZT value was about 0.13 around 1000 K for the Si-, Ge- and Sn-doped samples. The optimization of x for each $In_{2-x}M_xO_3$ system may enhance the P and ZT values further as indicated for the Ge diped sample shown in Fig. 5.

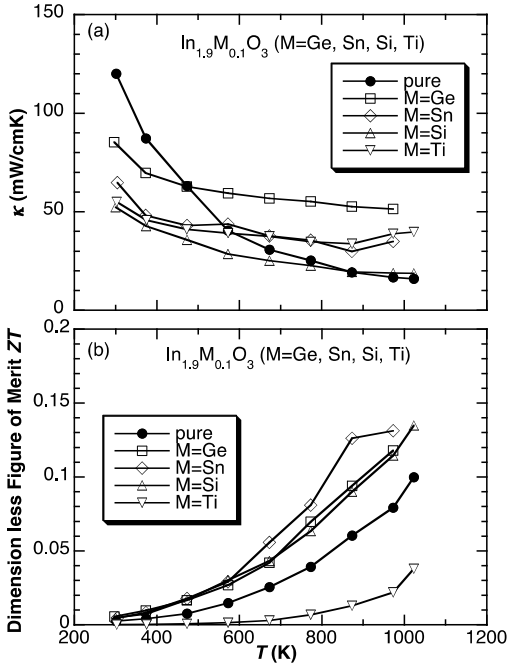

Fig. 10. Temperature dependence of the (a) thermal conductivity κ and (b) dimensionless figure of merit ZT of the $In_{1.9}M_{0.1}O_3$ (M=Si, Ti, Ge, Sn).

3.3 In_2O_3-SnO_2 system

In order to reduce the amount of the In metal, we investigated thermoelectric properties of the In_2O_3-SnO_2 system. SnO_2 shows similar physical properties to In_2O_3, which is inexpensive, plentiful and nontoxic, as a substitute for the expensive In_2O_3. Figure 11 shows the XRD patterns of the In_2O_3-SnO_2 samples with various mixing ratios. It was found that all the samples were the mixture of SnO_2 and In_2O_3 phases without other impurity phase.

Figure 12(a) shows the electrical resistivity ρ and Seebeck coefficient S at 1173 K for the In_2O_3-SnO_2 system, as a function of the fraction of SnO_2. As shown in the subsection of 3.2, the ρ value was decreased by two orders of magnitude by the 5% SnO_2 mixing in the $In_{1.9}Sn_{0.1}O_3$ sample, which results from the slight Sn^{4+} substitution for the In^{3+} site. As a result, electrons were doped in the sample and, at the same time, the $|S|$ value was also decreased. And then, the ρ and $|S|$ values increased with increasing the contents of the SnO_2 phase and approached those of the pristine SnO_2. The power factor P at 1173 K for the system, as a function of the fraction of SnO_2, is shown in Fig. 12(b). The P value took a maximum by the 5% SnO_2 mixture and then decreased with the increase in the fraction of SnO_2.

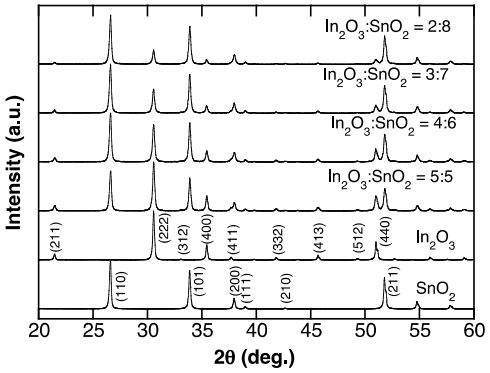

Fig. 11. XRD patterns of the In_2O_3-SnO_2.samples with various mixing ratios fabricated by SPS method.

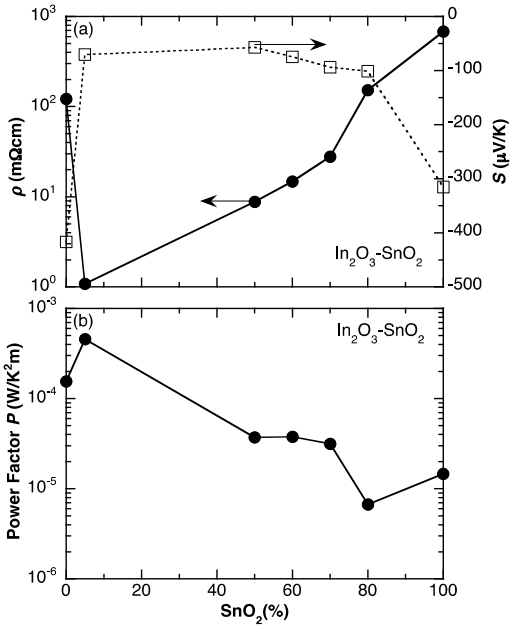

Fig. 12. (a) The resistivity ρ and Seebeck coefficient S and (b) power factor P of the In_2O_3-SnO_2 samples at 1173 K, as a function of the fraction of the SnO_2.

3.4 Sb doping to the In_2O_3-SnO_2 system

In order to introduce the carriers to the In_2O_3-SnO_2 system, pentavalent antimony (Sb^{5+}) was doped, which is expected to substitute both for In^{3+}- and Sn^{4+}-sites. First, we investigated the Sb doping effect to the In_2O_3. Figures 13(a) and 13(b) show the electrical resistivity ρ and Seebeck coefficient S of the $In_{2-x}Sb_xO_3$ (x=0.1), respectively. The ρ and $|S|$ values decreased with the Sb substitution, which suggests that Sb acts as a donor. Next, we investigated the Sb doping effect to the SnO_2. Figures 13(c) and 13(d) show the ρ and S values of the $Sn_{0.985-x}Sb_xZn_{0.015}O_2$, respectively. Since many cracks were created and the mass density was relatively low for the $Sn_{1-x}Sb_xO_2$, a small amount of ZnO (y=0.015) was added as an auxiliary agent, which is a conventional technique to fabricate ceramics [18]. As a result, the SnO_2 samples as high density as 90% of the ideal one without crack can be fabricated by the Zn addition. The ρ and $|S|$ values of the $Sn_{0.985-x}Sb_xZn_{0.015}O_2$ system decreased with increasing Sb substitution, which

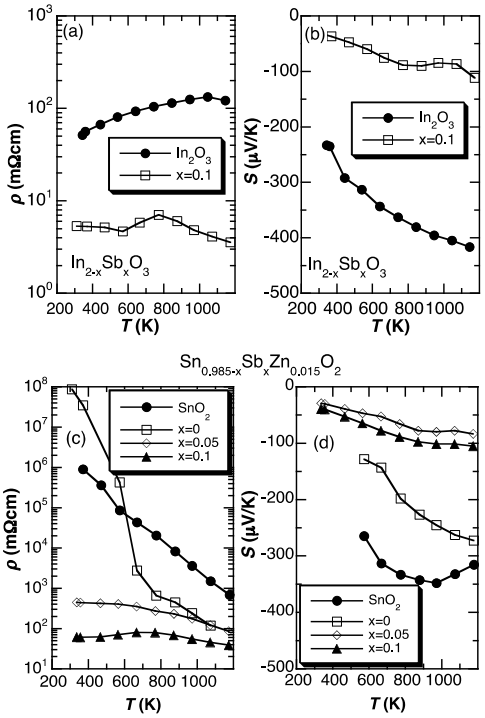

Fig. 13. Temperature dependence of the resistivity ρ and Seebeck coefficient S of $In_{2-x}Sb_xO_3$ ((a), (b)) and of $Sn_{0.985-x}Sb_xZn_{0.015}O_2$ ((c), (d)).

suggests that electrons were doped by the Sb substitution in the SnO_2 system.

The Sb doping was investigated for the In_2O_3-SnO_2 system. Figure 14(a) shows the XRD patterns of $(Sn_{0.5}In_{0.5})_{1-x-y}Sb_xZn_yO_2$ as a function of the Sb contents x, in which the ratio of the In_2O_3:SnO_2=1:1 was fixed as a typical example. The contents of ZnO were fixed to be y=0.02, which was slightly larger than y=0.015 shown in Figs. 13(c) and 13(d). The difference in the contents of auxiliary agent y was confirmed not to influence on the electrical properties. In Fig. 14(a), only the peaks of SnO_2 and In_2O_3 phases can be indexed without impurity, even though the Sb was doped up to x=0.06. Figures 14(b) and 14(c) show the magnification of the (110) XRD peak of SnO_2 phase and the (222) peak of In_2O_3 phase for each sample, respectively. It should be noted that the (222) peak of In_2O_3 shifts to higher angle with increasing the contents of Sb, but the (110) peak of SnO_2 hardly shifts. The ionic radius of In^{3+}, Sn^{4+} and Sb^{5+} is 0.80Å, 0.69Å and 0.60Å, respectively [16]. These results suggest that the Sb atom was preferentially substituted for the In-site rather than the Sn-site. Because the peak shift of the (222) peak of In_2O_3 to higher angle results from the decrease of lattice parameter. On the other hand, unchanged (110) peak of the SnO_2 phase suggested that the most of the doped Sb substituted for the In-site.

Figure 15 shows the temperature dependence of ρ, S and P values of the $(Sn_{0.5}In_{0.5})_{1-x-y}Sb_xZn_yO_2$ system. The lowest ρ value was realized for the $Sn_{0.5}In_{0.5}O_3$ sample because of the Sn substitution for the In-site. As a result, the $|S|$ value also decreased and the P value was not so high. Since the Sb atoms were expected to substitute mainly for the In-site as discussed in Fig. 14, the ρ value

slightly decreases with increasing Sb content. However, the P value of the substituted samples does not exceed that of In_2O_3.

Figures 16(a) and 16(b) depict the temperature dependence of the κ and ZT values of the typical $(Sn_{0.5}In_{0.5})_{1-x-y}Sb_xZn_yO_2$ samples, respectively. The κ value was fairly reduced at low temperatures by mixing the SnO_2, Sb and Zn into the parent In_2O_3 material. On the other hand, at higher temperatures, the phonon-phonon scattering for the pure In_2O_3 sample is dominant, compared to the impurity scattering in the other $(Sn_{0.5}In_{0.5})_{1-x-y}Sb_xZn_yO_2$ samples. The ZT of $(Sn_{0.5}In_{0.5})_{1-x-y}Sb_xZn_yO_2$ could not exceed that of the pure In_2O_3.

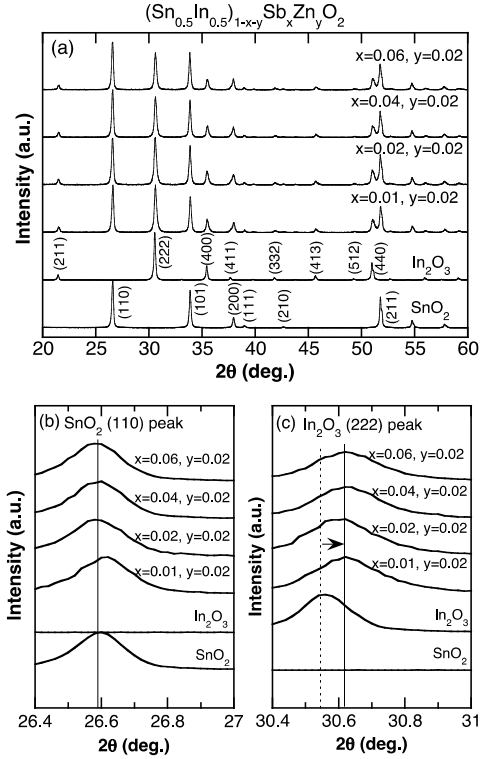

Fig. 14. (a) XRD patterns of the $(Sn_{0.5}In_{0.5})_{1-x-y}Sb_xZn_yO_2$., Enlarged views around the (b) (110) SnO_2 peak ($2\theta \sim 26.6°$) and (c) (222) In_2O_3 peak ($2\theta \sim 30.6°$).

4. SUMMARY

We have investigated the thermoelectric properties of the $In_{2-x}M_xO_3$ system doped with tetravalent elements (M=Si, Ti, Ge, Sn, Te, Ce) and those of the In_2O_3-SnO_2 system doped with pentavalent Sb element.

For the $In_{2-x}M_xO_3$ system, the maximum power factor $P=S^2/\rho$ and the maximum dimensionless figure of merit ZT were realized for the M=Ge sample, which suggest that the Ge is the best dopant. These results qualitatively reproduced those reported by Berardan *et al.*

For the In_2O_3-SnO_2 system doped with Sb^{5+}, which is proposed to reduce the amount of the expensive In, Sb atom was preferentially substituted for the In-site rather than the Sn-site. The P value of the samples does not exceed that of the pure In_2O_3, contrary to our expectation. Other substitution element and/or mixed system must be explored to enhance the thermoelectric performance of the In_2O_3 system.

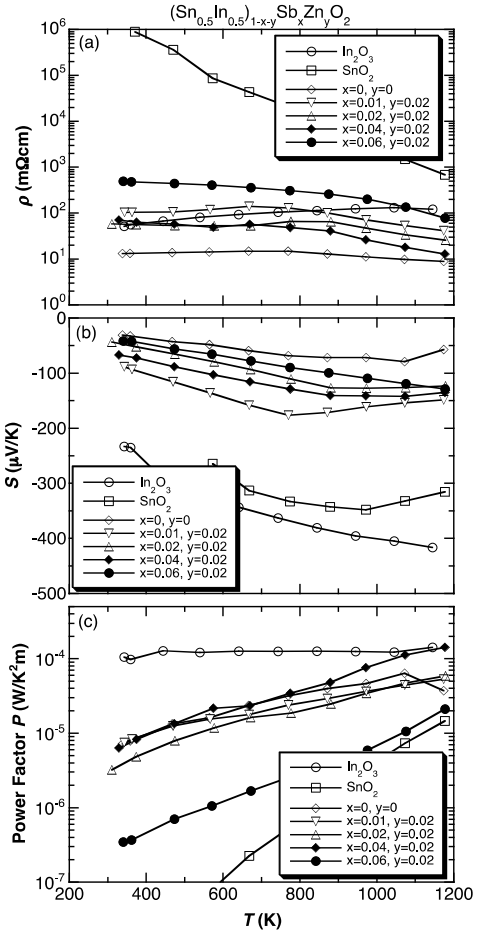

Fig. 15. Temperature dependence of (a) resistivity ρ, (b) Seebeck coefficient S and (c) power factor P of $(Sn_{0.5}In_{0.5})_{1-x-y}Sb_xZn_yO_2$ system.

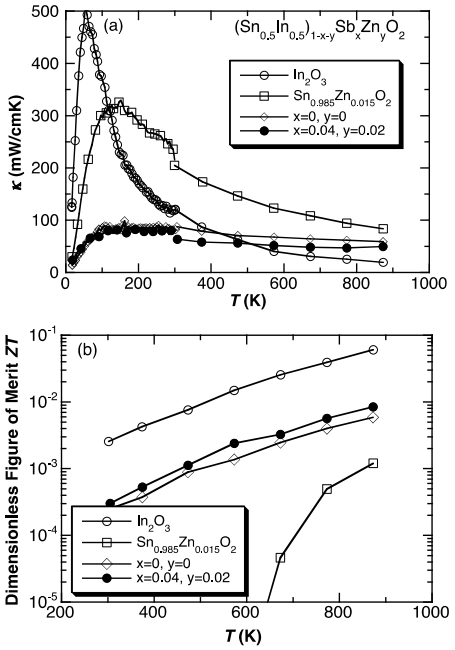

Fig. 16. Temperature dependence of (a) thermal conductivity κ, (b) dimensionless figure of merit ZT of $(Sn_{0.5}In_{0.5})_{1-x-y}Sb_xZn_yO_2$ system.

Acknowledgments

The authors thank Professor Takashi Goto and Dr. Hirokazu Katsui of Tohoku University, Japan, for the assistance in thermal conductivity measurement using laser flash method and for valuable discussion. This work was performed under the Inter-university Cooperative Research Program of the Institute for Materials Research, Tohoku University.

References

[1] I. Terasaki, Y. Sasago, and K. Uchinokura, *Phys. Rev*. B **56**, R12685-7 (1997).
[2] R. Funahashi, I. Matsubara, H. Ikuta, T. Takeuchi, U. Mizutani, and S. Sodeoka, *Jpn. J. Appl. Phys*. **39**, L1127-9 (2000).
[3] H. Muta, K. Kurosaki, and S. Yamanaka, *J. Alloys Compd*. **350**, 292-295 (2003).
[4] T. Tsubota, M. Ohtaki, K. Eguchi, and H. Arai, *J. Mater. Chem*. **8**, 409-412 (1998).
[5] D. Berardan, E. Guilmeau, A. Maignan, and B. Raveau, *Solid State Commun*., **146**, 97-101 (2008).
[6] Y. Lin, Y. Lin, J. Lan, W. Xu, B-P. Zhang, C-W. Nan and H. Zhu, J. Am. Ceram. Soc. 93, 2938-2941 (2010).
[7] M. Ohtaki, D. Ogura, K. Eguchi and H. Arai, *J. Mater. Chem*., **4**, 653-6 (1994).
[8] Y. Liu, Y. Lin, J. Lan, B-P. Zhang, W. Xu, C-W. Nan and H. Zhu, *J. Electron. Mat.* **40**, 1083-1086 (2011).
[9] B. Cheng, H. Fang, J. Lan, Y. Liu, Y-H. Lin and C-W. Nan, *J. Am. Ceram. Soc.* **94**, 2279-2281 (2011).
[10] J. Lan, Y. Liu, Y. Lin, C-W. Nan, Q. Cai and X. Yang, *Scientific Rep.* **5**, 7783 (2015).
[11] D. Berardan, E. Guilmeau, A. Maignan and B. Raveau, *J. Appl. Phys.* **104**, 064918 (2008).
[12] J. Lan, Y. Lin, Y. Liu, S. Xu and C-W. Nan, *J. Am. Ceram. Soc.* **95**, 2465-2469 (2012).
[13] E. Combe, E. Guilmeau, E. Savary, S. Marinel, R. Cloots, R. Funahashi and F. Boschini, *J. Euro. Ceram. Soc.* **35**, 145-151 (2015).
[14] F. Izumi and T. Ikeda, *Mater. Sci. Forum* **321-324**, 198-203 (2000).
[15] H. Fujishiro, M. Ikebe, T. Naito, K. Noto, S. Kobayashi, and S. Yoshizawa, *Jpn. J. Appl. Phys*. **33**, 4965-4970 (1994).
[16] R. D. Shannon, *Acta Cryst.* **A32**, 751-767 (1976).
[17] M. Marezio, *Acta Cryst.*, **20**, 723-8 (1966).
[18] S. Yanagiya, N. V. Nong, J. Xu, M. Sonne, and N. Pryds, *J. Electro. Mat.* **40**, 674-7 (2011).

(Received January 21, 2015; Accepted August 27, 2015)